ACS Medicinal Chemistry Letters

Letter

Cite This: ACS Med. Chem. Lett. 2018, 9, 832−837

Carbon Dots from Sugars and Ascorbic Acid: Role of the Precursors on Morphology, Properties, Toxicity, and Drug Uptake

Simone Cailotto,[†] Emanuele Amadio,*[,†] Manuela Facchin,[†] Maurizio Selva,[†] Enrico Pontoglio,[†] Flavio Rizzolio,[†,‡] Pietro Riello,[†] Giuseppe Toffoli,[‡] Alvise Benedetti,[†] and Alvise Perosa*[,†]

[†]Department of Molecular Sciences and Nanosystems, Università Ca' Foscari Venezia, Via Torino 155, 30172 Venezia Mestre, Italy

[‡]Experimental and Clinical Pharmacology Unit, C.R.O. National Cancer Institute, 33081 Aviano, Italy

Supporting Information

ABSTRACT: There is the need for reproducible, simple, high-yielding synthetic protocols aimed at obtaining carbon dots (CDs) with controlled fluorescence, photothermal and photochemical behavior, surface properties, biocompatibility, tumor targeting ability, drug absorption biodistribution, and tumor uptake. This Letter describes a systematic study on the effect of glucose, fructose, and ascorbic acid as starting materials for the preparation of highly luminescent CDs, characterized by a blue emission. Their composition and morphology are investigated by titration of OH surface groups, spectroscopic techniques, and high-resolution transmission electron microscopy (HR-TEM), and their toxicity was tested toward HeLa cells. CDs made using fructose were toxic, while those made from glucose and ascorbic acid showed good biocompatibility. The reproducible and simple synthetic procedure yields luminescent biomass-derived CDs for combined cancer therapy and diagnostics. Their doxorubicin (DOX) drug uptake was measured by spectrofluorimetry, indicating a crucial role of the morphologies of the CDs in controlling DOX loading. The glucose derived CDs showed up to 28% w/w of DOX loading.

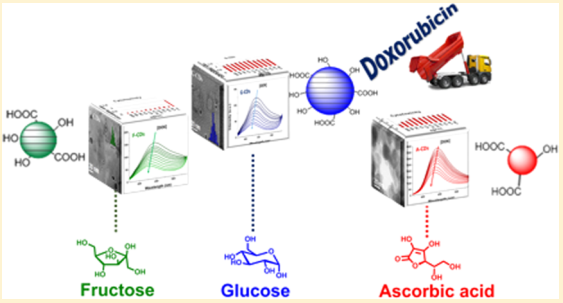

KEYWORDS: *Carbon dots, monosaccharides, biocompatible, nanocarriers, drug loading, doxorubicin*

Based on their optical, physical, chemical, and biological properties, carbon dots (CDs) have been proposed as nanotheranostic agents for combined cancer therapy and diagnostics.[1,2] Specifically, their high water solubility, biocompatibility, low toxicity, good cell permeability, excellent fluorescent imaging sensitivity, and easy conjugation with therapeutics indicate that CDs are ideal candidates as bioimaging probes and theranostic nanocarriers. Tailoring their design for clinical implementation implies the ability to control fluorescence, photothermal and photochemical behavior, biocompatibility, and drug absorption biodistribution and tumor uptake.[3−8] Before that, other issues that need to be carefully addressed are related to their synthesis and include batch-to-batch reproducibility, control of surface properties, purification, and characterization as we recently pointed out in this journal and elsewhere.[5,9,10] Full control and understanding of these features implies therefore a solid chemical background obtained by performing a systematic study of the starting materials, synthetic parameters, and of structure−property relationships. In this Letter, we took on this challenge and carried out the hydrothermal syntheses of CDs starting from a set of different reagents, followed by their morphological, chemical, and toxicological characterization and some preliminary structure−activity relationships as drug nanocarriers.

The method of our choice to produce CDs is hydrothermal;[11−13] it consists in heating an organic precursor in water, at high temperature and for a long time. With this method, it is possible to synthesize carbon nanoparticles from a variety of starting reagents: orange juice,[14] tea[5] or chocolate,[15] and protein[16] but also from other renewable resource like lignin,[17] willow bark[18] or cellulose, and waste paper.[19] Monosaccharides are another cheap, abundant, and biocompatible resource that can be used to obtain carbon dots with a high number of carboxylic groups on the surface, that in turn represent an important starting point for the development of efficient drug delivery systems. Very recently, by using doxorubicin (DOX) as a model anticancer drug, it has been demonstrated that noncovalent interactions (such as electrostatic interaction, hydrophobic interaction, $\pi-\pi$ stacking, and hydrogen bonding) are responsible for the binding of DOX to the CDs nanostructure.[20] Among the others, an important role is played by the native carboxyl groups on the CDs surface, which, by interaction with the amine moiety of DOX, led to the formation of pH responsive nanoaggregates employed for cancer-specific localized drug release.[6] A number of hydrothermal procedures for the synthesis of sugar-based CDs have been reported in the last decades, mainly in the presence of both passivating or doping agents like N or P.[21] Yang et al. synthesized CDs starting from glucose using PEG−200 as passivating agent achieving a

Received: May 25, 2018
Accepted: July 16, 2018
Published: July 16, 2018

DOI: 10.1021/acsmedchemlett.8b00240
ACS Med. Chem. Lett. 2018, 9, 832−837

nanomaterial with remarkable quantum yield (QY) of 6.3%.[22] Travas-Sejdic et al. reported a synthesis of CDs by simply refluxing glucose in sulfuric acid, forming carbon nanoparticles with poor QY (1%), which, by adding a passivating agent, could be raised up to 13%.[23] Wang et al. developed a synthesis of glucose-based CDs by using monopotassium phosphate as a dehydrating inorganic base to favor the formation of the nanoparticles.[24]

To favor the formation of biocompatible nanostructures suitable for medical applications and to avoid the formation of harmful chemical compounds, in this work we describe the hydrothermal synthesis of CDs starting from fructose, glucose, and ascorbic acid, without any passivating or doping additives. The as-synthesized CDs are here characterized from a morphological, chemical, and toxicological point of view and their potential application as drug nanocarriers are tested using DOX as a model drug. There are only few similar examples: for glucose and fructose, a microwave approach was reported,[25] while in the case of ascorbic acid, ethanol was added as a cosolvent.[26]

The **G−CDs**, **F−CDs**, and **A−CDs** were synthesized by thermolysis of an aqueous solution of glucose, fructose, or ascorbic acid at 200 °C for 24 h in autoclave (see Supporting Information (SI) for details). The morphology and structural features of the CDs were investigated by NMR, mass spectrometry (GC−MS), Fourier transform infrared spectroscopy (FT−IR), UV−vis spectroscopy, and high-resolution-transmission electron microscopy (HR-TEM). ^{1}H and ^{13}C{^{1}H} NMR spectra (Figure S1−3) reveal the disappearance of the reagent and the formation of NMR-active compounds, indicative of the presence of both alkyl and/or aromatic functionalities. For the **F−CDs**, furan-like molecules such as hydroxymethylfurfural **1** and 2,5-furandicarboxaldehyde **2** were identified by GC−MS (Figures S4−S6) and ^{1}H and the ^{13}C NMR (Figure S7). Dehydration to yield furan-like molecules in the thermal degradation of carbohydrates is well-known.[27−29] Furanics are carcinogenic, this must be kept in mind when considering CDs for biomedical purposes. Instead, silent GC−MS spectra were observed for both **G−CDs** and **A−CDs**.

Diffusion-ordered NMR spectroscopy (DOSY) was used to estimate the size of the CDs. By assuming spherical ideal structures, by comparison with a known reference, and according to the Stokes−Einstein equation and Graham's law of diffusion, the diffusion coefficient (Δ) estimated using DOSY allows to calculate a relative volume ($\bar{\varepsilon}$) and mass ($\bar{M}$) and, thus to estimate the MW of the CDs (see SI for more details).[30−32] In Figure 1 (see also Figures S8−10), the DOSY spectra of the three CDs are reported in comparison with the ones of the organic precursors, which have been used as reference. Interestingly, the analyses reveal that the CDs are effectively larger than the corresponding precursors, and despite the identical hydrothermal conditions applied during the synthesis, their actual dimension depends on the reagent used, being **G−CDs** larger than the **F−CDs** and **A−CDs**. As reported in Table 1

Table 1. Average Volume ($\bar{\varepsilon}$), Mass Ratios ($\bar{M}$), and Estimated Molecular Mass ($\overline{MW}$) of the CDs[a]

CDs	$\bar{\varepsilon}$	$\bar{M}$	$\overline{MW}$
G-CDs	55.7	14.6	2600 ± 120
F-CDs	22.0	7.8	1400 ± 160
A-CDs	13.4	5.6	990 ± 70

[a]Normalized to the corresponding substrate (c.f.r. Supporting Info).

(see also Table S1 for more details), **F−CDs** and **G−CDs** are up to 25−60 times larger and 9−15 times heavier than their respective precursors fructose/glucose. Their calculated MW are in the range between 2700 and 1500 Da, which is consistent with the formation of extended carbon nanostructures. For **A−CDs**, the higher Δ value obtained is reasonably ascribed to the presence in solution of small oligomeric structures. Typically, DOSY is used to study well-defined molecular-like species,[33−35] while the present solutions contain highly complex systems formed by a mixture of different carbogenic frameworks, rather than a single molecule. For this reason, the present data for such "nonideal" samples is purely indicative of the average molecular weight of the CDs and is underestimated due to the fact that DOSY provides a weighted average of the mass of the ^{1}H NMR active species.

The CDs were then characterized by FT−IR (Figure S11). All three samples showed intense adsorption bands indicative of C═C conjugated aromatics,[36] C═O bonds, OH groups, C−H bonds, and C−O−C moieties.[37] High-resolution transmission electron microscopy (HR-TEM) of the **G−CDs** and **F−CDs** revealed the presence of homogeneous and well-dispersed populations of small quasi-spherical nanoparticles with an average size of 9−10 nm with a polydispersity index (PDI) of 0.025−0.03 indicative of monodisperse systems (Figure 2). Furthermore, the HR-TEM images of the **G−CDs** and **F−CDs** showed the presence of lattice fringes with an interlayer spacing of 2.4 Å, confirming their graphitic nature. Instead, the **A−CDs** showed amorphous and poorly defined structures confirming their molecular-like nature in agreement with the DOSY results.

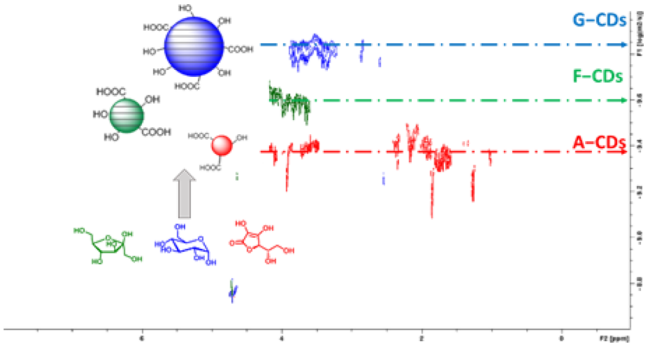

Figure 1. DOSY spectra in D_2O at pD = 7 of the **G−CDs**, **F−CDs**, and **A−CDs** [5 mg/mL].

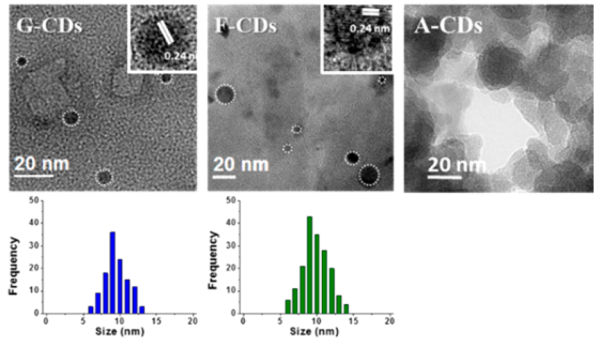

Figure 2. HR-TEM of the as-synthesized **G−CDs**, **F−CDs**, and **A−CDs**.

DOI: 10.1021/acsmedchemlett.8b00240
ACS Med. Chem. Lett. 2018, 9, 832−837

To shed light on the surface structure of the CDs, a titration[38] of the hydroxyl groups was carried out. The hydroxyl value (HV), *i.e.*, the grams of KOH required to neutralize 1 g of CDs (c.f.r. SI), was measured for the three different CDs. The results are reported in Figure S12. Both **F−CDs** and **G−CDs** showed a similar HV ≈ 1500, corresponding to 26.8 mol(OH)/g(CD). This is not surprising since the chemical structure of the precursors and their derived CDs are very similar. This low HV was explained by the observation that the hydrothermal degradation of glucose and fructose produced large amounts of CO_2 and H_2O, with concurrent formation of extended carbogenic structures. The higher HV ≈ 5000 of the **A−CDs**, corresponding to 89.3 mol(OH)/g(CD), reflects instead the low degree of carbonization and the consequent presence of free carboxyl-rich molecules in solution. Based on these observation, an investigation of the surface charge of the nanoparticles was carried out by electrophoresis. The images are shown in Figure 3. It is readily apparent that in the pH range 4−10, all the CDs

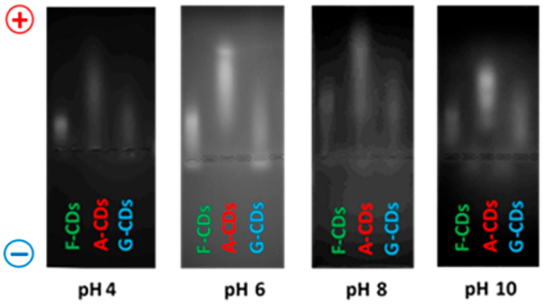

Figure 3. Electrophoresis experiment performed on the **G−CDs**, **F−CDs**, and **A−CDs** at different pHs.

were negatively charged in agreement with the presence of hydroxyl and carboxylic groups on the surface. The HV values of each sample correlate with the electrophoresis: the higher the negative surface charge, the faster the migration toward the positive electrode.

The optical properties of the carbon dots were investigated by UV−Vis absorption spectroscopy and by recording the photoluminescence (PL) spectra (Figure 4). UV−Vis spectra showed a common absorption band for the three different CDs in the region of 225−235 nm ascribed to the $\pi-\pi^*$ transition of the sp^2 C═C conjugated system. The **G−CDs** and **F−CDs** showed absorption peaks also at 265 and 280 nm, respectively, ascribed to the $n-\pi^*$ transition of the C═O groups on the surface.[39] Moreover, the **F−CDs** showed an absorption peak at 360 nm for the transition associated with the trapping of excited-state energy by the surface state.[40] As shown in Figure 4, in all three samples, the emission spectra were analyzed at different excitation wavelengths: 330−380 nm. Despite the similarity of the starting materials, not all samples showed emission dependence from the excitation wavelength. Indeed, when the excitation wavelength was shifted from 330 to 380 nm, the emission peaks of **A−CDs** and **G−CDs** were red-shifted from 440 to 460 nm and from 435 to 450 nm, respectively. While no appreciable variation on the emission peaks were observed for **F−CDs**. This phenomenon could be ascribed to a size-dependent emission,[41] or to the presence of fluorophores or structural defects on the surface.[42−44] The QYs of the CDs, calculated using quinine sulfate as standard, were 1.8%, 0.3%, and 1.5% for the **G−CDs**, **F-CDs**, and **A−CDs**, respectively. As expected, low QY were measured in all cases due to the absence of doping atoms (e.g., N or P)[45] and of passivation agents as well as to the presence of defects and conjugated carbon core domains, which favor nonradiative electron−hole recombination pathways.[46]

The carbon nanoparticles were then tested for their toxicity toward HeLa cells in view of a potential use in the nanomedical field. The cell viability was measured at different CDs concentrations with respect to a control suspension; the results are summarized in Figure 5. The **G−CDs** showed good viability at all the concentrations tested. Instead, the **A−CDs** showed biocompatibility only at relatively low concentration (<250 μg/mL). The **F−CDs** exhibited high toxicity also at low concentrations, explained by the presence of the furanics identified earlier in the **F−CDs** mixture, which are known to be carcinogenic.[47,48]

The interactions of the three different CDs with DOX were measured by fluorescence quenching in view of the future development of new biocompatible delivery systems. DOX was gradually added to a solution of CDs (0.25 mg/mL) while keeping the CDs concentration constant. The results shown in Figure 6 clearly demonstrate that the gradual addition of DOX (from 1×10^{-6} to 1×10^{-5} M) induces a progressive decrease of the fluorescence intensity that can be attributed to dynamic or static interactions between the CDs and DOX.[49,50] The blue-shift of the emission peak indicates a strong interaction.[51] The CDs−DOX association constants (K_{sv}), calculated with the Stern−Volmer plots shown in Figure 7 (c.f.r. SI), exhibit linear relationships meaning that dynamic quenching process are involved. **F−CDs** and **G−CDs** show a similar K_{sv}, while the **A−CDs** exhibit an interaction half of that. The high HV value of the **A−CDs** could have been expected to favor association with DOX by electrostatic interactions. The Stern−Volmer plots indicate the opposite, i.e, that noncovalent interactions are controlling the adsorption of the drug. A role may be played by $\pi-\pi$ stacking between the graphitic carbon core in the **F−CDs** and **G−CDs**, with the aromatic moiety of DOX.[17] DOX uptake by **G−CDs**, chosen for its high drug affinity and low toxicity, was estimated by constructing a Job plot of the fluorescence emission quenching (λ_{ex} = 340 nm, λ_{em} = 441 nm) as a function

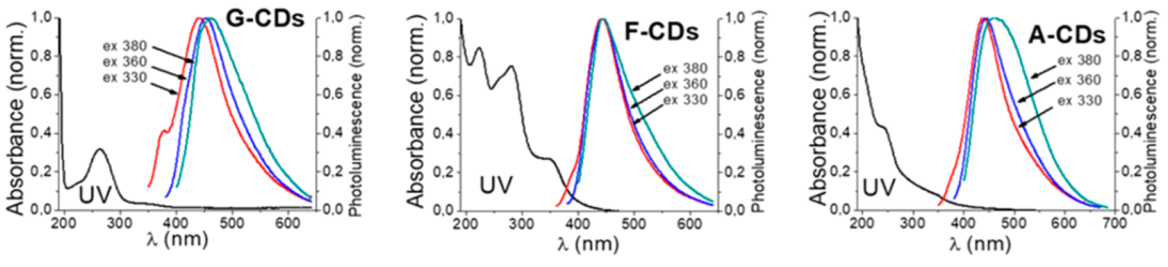

Figure 4. UV−vis spectra and PL spectra at different excitation wavelength of **G−CDs**, **F−CDs**, and **A−CDs** (50 μg/mL).

DOI: 10.1021/acsmedchemlett.8b00240
ACS Med. Chem. Lett. 2018, 9, 832−837

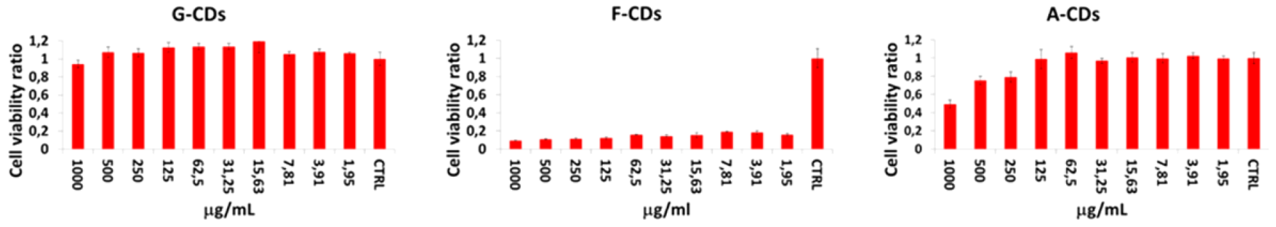

Figure 5. Cell viability ratio of the CDs.

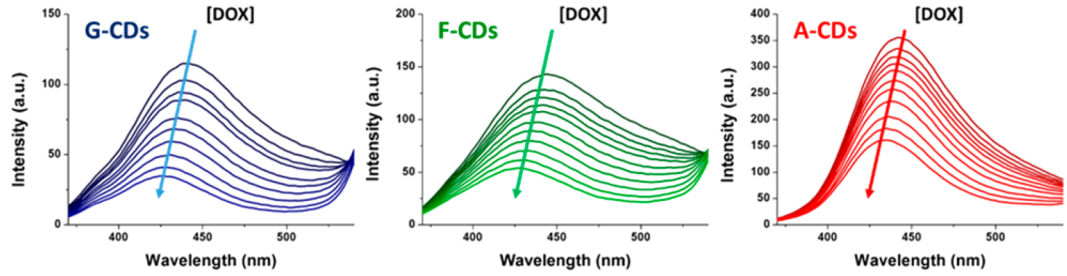

Figure 6. Emission spectra of CDs (0.25 mg/mL) recorded at different addition of DOX (from 1×10^{-6} to 1×10^{-5} M).

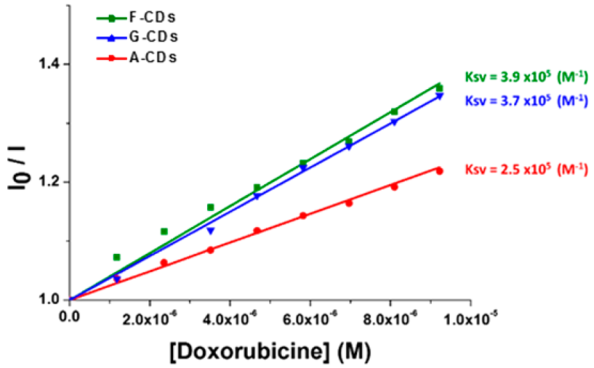

Figure 7. Stern–Volmer plots of the relative emission intensities (λ_{ex} = 340 nm λ_{em} = 441 nm) of CDs (0.25 mg/mL) as a function of the DOX concentration.

of DOX relative mass fraction ($m_{DOX}/[m_{DOX} + m_{CDs}]$) (Figure 8). The plot reveals a binding stoichiometry **G–CDs**/DOX of ca. 3.5:1 that leads to a calculated drug loading of 28%$_{w/w}$, comparable or higher than the most efficient doped or functionalized analogs.[52,53]

In conclusion, we have shown how the choice of the reagents influences the morphology, structure, and properties of the obtained CDs and how these correlate with the drug loading capabilities. In particular, the fluorescence quenching measurements revealed the importance of the graphitic core domains in achieving high CDs–DOX affinity as evinced by the binding trend. Drug delivery test are currently being performed.

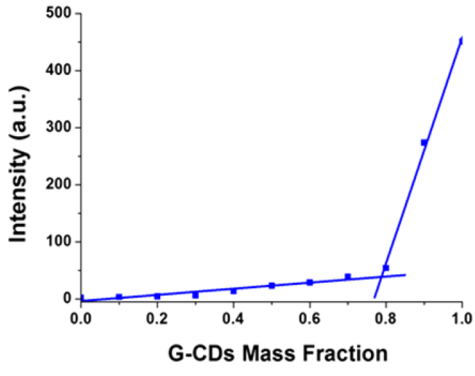

Figure 8. Job plot of the fluorescence decay (λ_{ex} = 340 nm λ_{em} = 440 nm) of **G-CDs** with DOX.

■ ASSOCIATED CONTENT

Supporting Information

The Supporting Information is available free of charge on the ACS Publications website at DOI: 10.1021/acsmedchemlett.8b00240.

Materials and instrumentations, syntheses of the carbon dots, hydroxyl value (HV) quantification, CDs–doxorubicin interaction quenching, ^{1}H and ^{13}C NMR spectra and DOSY of CDs, IR characterization and HV values, and polydispersity index (PDF)

■ AUTHOR INFORMATION

Corresponding Authors

*E-mail: emanuele.amadio@unive.it.
*E-mail: alvise@unive.it.

ORCID

Maurizio Selva: 0000-0002-9986-2393
Flavio Rizzolio: 0000-0002-3400-4363
Alvise Perosa: 0000-0003-4544-8709

Author Contributions

A.P., E.A., and S.C. conceived the experiments and wrote the paper. S.C. and E.P. performed the experiments; M.F., M.S., F.R., P.R., G.T., and A.B. contributed to the interpretation of results.

Notes

The authors declare no competing financial interest.

■ ACKNOWLEDGMENTS

E.A. thanks the European Social Fund for a scholarship.

■ REFERENCES

(1) Lim, S. Y.; Shen, W.; Gao, Z. Carbon quantum dots and their applications. *Chem. Soc. Rev.* **2015**, *44*, 362–381.

DOI: 10.1021/acsmedchemlett.8b00240
ACS Med. Chem. Lett. 2018, 9, 832–837

(2) Wang, Y.; Hu, A. Carbon quantum dots: synthesis, properties and applications. *J. Mater. Chem. C* **2014**, *2*, 6921.
(3) Zhao, A.; Chen, Z.; Zhao, C.; Gao, N.; Ren, J.; Qu, X. Recent advances in bioapplications of C-dots. *Carbon* **2015**, *85*, 309−327.
(4) Feng, T.; Ai, X.; An, G.; Yang, P.; Zhao, Y. Charge-Convertible Carbon Dots for Imaging-Guided Drug Delivery with Enhanced in Vivo Cancer Therapeutic Efficiency. *ACS Nano* **2016**, *10*, 4410−4420.
(5) Bayda, S.; Hadla, M.; Palazzolo, S.; Kumar, V.; Caligiuri, I.; Ambrosi, E.; Pontoglio, E.; Agostini, M.; Tuccinardi, T.; Benedetti, A.; Riello, P.; Canzonieri, V.; Corona, G.; Toffoli, G.; Rizzolio, F. Bottom-up synthesis of carbon nanoparticles with higher doxorubicin efficacy. *J. Controlled Release* **2017**, *248*, 144−152.
(6) Zeng, Q.; Shao, D.; He, X.; Ren, Z.; Ji, W.; Shan, C.; Qu, S.; Li, J.; Chen, L.; Li, Q. Carbon dots as a trackable drug delivery carrier for localized cancer therapy in vivo. *J. Mater. Chem. B* **2016**, *4*, 5119−5126.
(7) Wang, Q.; Huang, X.; Long, Y.; Wang, X.; Zhang, H.; Zhu, R.; Liang, L.; Teng, P.; Zheng, H. Hollow luminescent carbon dots for drug delivery. *Carbon* **2013**, *59*, 192−199.
(8) Mosconi, D.; Mazzier, D.; Silvestrini, S.; Privitera, A.; Marega, C.; Franco, L.; Moretto, A. Synthesis and Photochemical Applications of Processable Polymers Enclosing Photoluminescent Carbon Quantum Dots. *ACS Nano* **2015**, *9*, 4156−4164.
(9) Kumar, V.; Toffoli, G.; Rizzolio, F. Fluorescent Carbon Nanoparticles in Medicine for Cancer Therapy. *ACS Med. Chem. Lett.* **2013**, *4*, 1012−1013.
(10) Rani, R.; Kumar, V.; Rizzolio, F. Fluorescent Carbon Nanoparticles in Medicine for Cancer Therapy: An Update. *ACS Med. Chem. Lett.* **2018**, *9*, 4−5.
(11) Jiang, K.; Sun, S.; Zhang, L.; Lu, Y.; Wu, A.; Cai, C.; Lin, H. Red, Green, and Blue Luminescence by Carbon Dots: Full-Color Emission Tuning and Multicolor Cellular Imaging. *Angew. Chem., Int. Ed.* **2015**, *54*, 5360−5363.
(12) Sun, Y.-P.; Zhou, B.; Lin, Y.; Wang, W.; Fernando, K. A. S.; Pathak, P.; Meziani, M. J.; Harruff, B. A.; Wang, X.; Wang, H.; Luo, P. G.; Yang, H.; Kose, M. E.; Chen, B.; Veca, L. M.; Xie, S.-Y. Quantum-Sized Carbon Dots for Bright and Colorful Photoluminescence. *J. Am. Chem. Soc.* **2006**, *128*, 7756−7757.
(13) Yang, Z.; Li, Z.; Xu, M.; Ma, Y.; Zhang, J.; Su, Y.; Gao, F.; Wei, H.; Zhang, L. Controllable Synthesis of Fluorescent Carbon Dots and Their Detection Application as Nanoprobes. *Nano-Micro Lett.* **2013**, *5*, 247−259.
(14) Sahu, S.; Behera, B.; Maiti, T. K.; Mohapatra, S. Simple one-step synthesis of highly luminescent carbon dots from orange juice: application as excellent bio-imaging agents. *Chem. Commun.* **2012**, *48*, 8835−8837.
(15) Liu, Y.; Zhou, Q.; Li, J.; Lei, M.; Yan, X. Selective and sensitive chemosensor for lead ions using fluorescent carbon dots prepared from chocolate by one-step hydrothermal method. *Sens. Actuators, B* **2016**, *237*, 597−604.
(16) Zhang, Z.; Hao, J.; Zhang, J.; Zhang, B.; Tang, J. Protein as the source for synthesizing fluorescent carbon dots by a one-pot hydrothermal route. *RSC Adv.* **2012**, *2*, 8599−8601.
(17) Chen, W.; Hu, C.; Yang, Y.; Cui, J.; Liu, Y. Rapid Synthesis of Carbon Dots by Hydrothermal Treatment of Lignin. *Materials* **2016**, *9*, 184.
(18) Qin, X.; Lu, W.; Asiri, A. M.; Al-Youbi, A. O.; Sun, X. Green, low-cost synthesis of photoluminescent carbon dots by hydrothermal treatment of willow bark and their application as an effective photocatalyst for fabricating Au nanoparticles-reduced graphene oxide nanocomposites for glucose detection. *Catal. Sci. Technol.* **2013**, *3*, 1027−1035.
(19) Adolfsson, K. H.; Hassanzadeh, S.; Hakkarainen, M. Valorization of cellulose and waste paper to graphene oxide quantum dots. *RSC Adv.* **2015**, *5*, 26550−26558.
(20) Peng, Z.; Han, X.; Li, S.; Al-Youbi, A. O.; Bashammakh, A. S.; El-Shahawi, M. S.; Leblanc, R. M. Carbon dots: Biomacromolecule interaction, bioimaging and nanomedicine. *Coord. Chem. Rev.* **2017**, *343*, 256−277.
(21) Hill, S.; Galan, M. C. Fluorescent carbon dots from mono- and polysaccharides: synthesis, properties and applications. *Beilstein J. Org. Chem.* **2017**, *13*, 675−693.
(22) Zhu, H.; Wang, X.; Li, Y.; Wang, Z.; Yang, F.; Yang, X. Microwave synthesis of fluorescent carbon nanoparticles with electrochemiluminescence properties. *Chem. Commun.* **2009**, *34*, 5118.
(23) Peng, H.; Travas-Sejdic, J. Simple Aqueous Solution Route to Luminescent Carbogenic Dots from Carbohydrates. *Chem. Mater.* **2009**, *21*, 5563−5565.
(24) Yang, Z.-C.; Wang, M.; Yong, A. M.; Wong, S. Y.; Zhang, X.-H.; Tan, H.; Chang, A. Y.; Li, X.; Wang, J. Intrinsically fluorescent carbon dots with tunable emission derived from hydrothermal treatment of glucose in the presence of monopotassium phosphate. *Chem. Commun.* **2011**, *47*, 11615−11617.
(25) Tang, L.; Ji, R.; Cao, X.; Lin, J.; Jiang, H.; Li, X.; Teng, K. S.; Luk, C. M.; Zeng, S.; Hao, J.; Lau, S. P. Deep Ultraviolet Photoluminescence of Water-Soluble Self-Passivated Graphene Quantum Dots. *ACS Nano* **2012**, *6*, 5102−5110.
(26) Zhang, B.; Liu, C. y.; Liu, Y. A Novel One-Step Approach to Synthesize Fluorescent Carbon Nanoparticles. *Eur. J. Inorg. Chem.* **2010**, *2010*, 4411−4414.
(27) Fan, X.; Huang, L.; Sokorai, K. J. B. Factors Affecting Thermally Induced Furan Formation. *J. Agric. Food Chem.* **2008**, *56*, 9490−9494.
(28) Ames, J. M. Control of the Maillard reaction in food systems. *Trends Food Sci. Technol.* **1990**, *1*, 150−154.
(29) Laroque, D.; Inisan, C.; Berger, C.; Vouland, É.; Dufossé, L.; Guérard, F. Kinetic study on the Maillard reaction. Consideration of sugar reactivity. *Food Chem.* **2008**, *111*, 1032−1042.
(30) Cohen, Y.; Avram, L.; Frish, L. Diffusion NMR Spectroscopy in Supramolecular and Combinatorial Chemistry: An Old Parameter—New Insights. *Angew. Chem., Int. Ed.* **2005**, *44*, 520−554.
(31) Fielden, J.; Long, D.-l.; Slawin, A. M. Z.; Kögerler, P.; Cronin, L. Ligand and Counterion Control of Ag(I) Architectures: Assembly of a {Ag8} Ring Cluster Mediated by Hydrophobic and Ag···Ag Interactions. *Inorg. Chem.* **2007**, *46*, 9090−9097.
(32) Macchioni, A.; Ciancaleoni, G.; Zuccaccia, C.; Zuccaccia, D. Determining accurate molecular sizes in solution through NMR diffusion spectroscopy. *Chem. Soc. Rev.* **2008**, *37*, 479−489.
(33) Consiglio, G.; Failla, S.; Finocchiaro, P.; Oliveri, I. P.; Purrello, R.; Di Bella, S. Supramolecular Aggregation/Deaggregation in Amphiphilic Dipolar Schiff-Base Zinc(II) Complexes. *Inorg. Chem.* **2010**, *49*, 5134−5142.
(34) Consiglio, G.; Failla, S.; Finocchiaro, P.; Oliveri, I. P.; Bella, S. D. Aggregation properties of bis(salicylaldiminato)zinc(ii) Schiff-base complexes and their Lewis acidic character. *Dalton T* **2012**, *41*, 387−395.
(35) Pilone, A.; Lamberti, M.; Mazzeo, M.; Milione, S.; Pellecchia, C. Ring-opening polymerization of cyclic esters by phenoxy-thioether complexes derived from biocompatible metals. *Dalton T* **2013**, *42*, 13036−13047.
(36) Loo, A. H.; Sofer, Z.; Bouša, D.; Ulbrich, P.; Bonanni, A.; Pumera, M. Carboxylic Carbon Quantum Dots as a Fluorescent Sensing Platform for DNA Detection. *ACS Appl. Mater. Interfaces* **2016**, *8*, 1951−1957.
(37) Wang, H.; Lu, Q.; Hou, Y.; Liu, Y.; Zhang, Y. High fluorescence S, N co-doped carbon dots as an ultra-sensitive fluorescent probe for the determination of uric acid. *Talanta* **2016**, *155*, 62−69.
(38) Hartman, L.; Lago, R. C. A.; Azeredo, L. C.; Azeredo, M. A. A. Determination of hydroxyl value in fats and oils using an acid catalyst. *Analyst* **1987**, *112*, 145−147.
(39) Xue, M.; Zhang, L.; Zhan, Z.; Zou, M.; Huang, Y.; Zhao, S. Sulfur and nitrogen binary doped carbon dots derived from ammonium thiocyanate for selective probing doxycycline in living cells and multicolor cell imaging. *Talanta* **2016**, *150*, 324−330.
(40) Gong, Y.; Yu, B.; Yang, W.; Zhang, X. Phosphorus, and nitrogen co-doped carbon dots as a fluorescent probe for real-time measurement of reactive oxygen and nitrogen species inside macrophages. *Biosens. Bioelectron.* **2016**, *79*, 822−828.

DOI: 10.1021/acsmedchemlett.8b00240
ACS Med. Chem. Lett. 2018, 9, 832−837

(41) Zhao, Q.-L.; Zhang, Z.-L.; Huang, B.-H.; Peng, J.; Zhang, M.; Pang, D.-W. Facile preparation of low cytotoxicity fluorescent carbon nanocrystals by electrooxidation of graphite. *Chem. Commun.* **2008**, 5116−5118.
(42) Sciortino, A.; Marino, E.; Dam, B. v.; Schall, P.; Cannas, M.; Messina, F. Solvatochromism Unravels the Emission Mechanism of Carbon Nanodots. *J. Phys. Chem. Lett.* **2016**, *7*, 3419−3423.
(43) Ju, B.; Nie, H.; Liu, Z.; Xu, H.; Li, M.; Wu, C.; Wang, H.; Zhang, S. X.-A. Full-colour carbon dots: integration of multiple emission centres into single particles. *Nanoscale* **2017**, *9*, 13326−13333.
(44) Pan, L.; Sun, S.; Zhang, A.; Jiang, K.; Zhang, L.; Dong, C.; Huang, Q.; Wu, A.; Lin, H. Truly Fluorescent Excitation-Dependent Carbon Dots and Their Applications in Multicolor Cellular Imaging and Multidimensional Sensing. *Adv. Mater.* **2015**, *27*, 7782−7787.
(45) Zhou, J.; Zhou, H.; Tang, J.; Deng, S.; Yan, F.; Li, W.; Qu, M. Carbon dots doped with heteroatoms for fluorescent bioimaging: a review. *Microchim. Acta* **2017**, *184*, 343−368.
(46) Fang, Q.; Dong, Y.; Chen, Y.; Lu, C.-H.; Chi, Y.; Yang, H.-H.; Yu, T. Luminescence origin of carbon based dots obtained from citric acid and amino group-containing molecules. *Carbon* **2017**, *118*, 319−326.
(47) Huang, X.; Duan, H.; Barringer, S. A. Effects of buffer and temperature on formation of furan, acetic acid and formic acid from carbohydrate model systems. *LWT - Food Science and Technology* **2011**, *44*, 1761−1765.
(48) Tong, X.; Ma, Y.; Li, Y. Biomass into chemicals: Conversion of sugars to furan derivatives by catalytic processes. *Appl. Catal., A* **2010**, *385*, 1−13.
(49) Valeur, B.; Berberan-Santos, M. N. Effects of Intermolecular Photophysical Processes on Fluorescence Emission. In *Molecular Fluorescence*; Wiley-VCH Verlag GmbH & Co. KGaA: 2012; pp 141−179.
(50) Lakowicz, J. *Principles of Fluorescence Spectroscopy*; Springer: 2006; Vol. *1*.
(51) Song, Y.; Zhu, S.; Xiang, S.; Zhao, X.; Zhang, J.; Zhang, H.; Fu, Y.; Yang, B. Investigation into the fluorescence quenching behaviors and applications of carbon dots. *Nanoscale* **2014**, *6*, 4676−4682.
(52) Gong, X.; Zhang, Q.; Gao, Y.; Shuang, S.; Choi, M. M. F.; Dong, C. Phosphorus and Nitrogen Dual-Doped Hollow Carbon Dot as a Nanocarrier for Doxorubicin Delivery and Biological Imaging. *ACS Appl. Mater. Interfaces* **2016**, *8*, 11288−11297.
(53) Wang, H.; Di, J.; Sun, Y.; Fu, J.; Wei, Z.; Matsui, H.; Alonso, A. d. C.; Zhou, S. Biocompatible PEG-Chitosan@Carbon Dots Hybrid Nanogels for Two-Photon Fluorescence Imaging, Near-Infrared Light/pH Dual-Responsive Drug Carrier, and Synergistic Therapy. *Adv. Funct. Mater.* **2015**, *25*, 5537−5547.

DOI: 10.1021/acsmedchemlett.8b00240
ACS Med. Chem. Lett. 2018, 9, 832−837